Influence of Concentration and pH of Hexafluorozirconic Acid on Corrosion Resistance of Anodized AA7075-T6

Jéssica Salles Pinheiro[1]* *, Gabriel Regio[1], Henrique Ribeiro Piaggio Cardoso[1],*

Claudia Trindade Oliveira[2], Jane Zoppas Ferreira[1]

[1]Programa de Pós-Graduação em Engenharia de Minas, Metalúrgica e de Materiais - PPGE3M, Universidade Federal do Rio Grande do Sul, Porto Alegre, RS, Brasil
[2]Instituto de Ciências Exatas e Tecnológicas, Universidade Feevale, Novo Hamburgo, RS, Brasil

7XXX aluminum alloys show high mechanical resistance and low weight, both required properties for aircraft industry. Anodizing is an electrolytical process typically used to improve the corrosion resistance of aluminum alloys, through which a thicker and porous oxide is formed. Boiling water is used as a common sealing method to the anodic layer; however, it implies energy expenditure. In this work, a two-step coating system was performed: anodizing in tartaric-sulphuric acid and a post-treatment with a Zr-based conversion coating, obtained at room temperature by immersion in hexafluorozirconic acid (H_2ZrF_6). To establish the best condition for coating formation on the aluminum oxide layer, different concentration and pH values of the H_2ZrF_6 solution were studied. Morphological and chemical analyses were performed respectively by SEM and EDS. The corrosion resistance evaluation was carried out by EIS in 0.5 M NaCl. Heterogeneity was observed in the obtained coatings. However, the samples treated with H_2ZrF_6 had a higher corrosion resistance than unsealed samples. The best concentration and pH range observed for the H_2ZrF_6 solution were 1 % and 3 to 3.5, respectively. Under these conditions, a greater corrosion resistance was evidenced in comparison to that obtained with boiling water sealing.

Keywords: *corrosion, anodizing, conversion coating, EIS.*

1. Introduction

Aluminum alloys from the 7000 series, which contain mainly Zn and Mg as alloy elements, have been used for years by the aircraft industry. These alloys show a high structural performance allied to low densities [1]. However, due to the heat treatment to increase their mechanical resistance, these alloys become susceptible to localized corrosion. Therefore, advanced surface protection methods are required [2]. Conversion coatings based on Cr(VI) ions have been widely used by the industry as they provide excellent corrosion resistance at low costs [3]. Nevertheless, these ions are toxic to human health and to the environment. Consequently, surface treatments based on Cr(VI) are already forbidden in the USA and the European Union [4,5]. On the other hand, Cr(III) ions represent less environmental and human health risks. Therefore, conversion coatings based on these ions have been adopted as replacements for those with Cr(VI)[6,7].

Another protection method for aluminum and its alloys consists of anodizing, which is another conversion coating, in which through an acidic medium and with the application of a current or potential, an alumina porous layer is obtained. This layer is able to increase corrosion resistance [8], besides enabling the anchorage of other coatings [9]. Chromic acid is widely used in the aircraft industry for Al alloys, as it provides suitable corrosion protection and adhesion properties for painting. However, for the same environmental issues

of Cr(VI) ions, this electrolyte has been replaced by mixed organic-inorganic acid baths such as tartaric-sulfuric, which produces oxide layers with comparable corrosion resistance to those produced in chromic baths and compatible to aerospace industry requirements [10–12].

Among the different sealing techniques used by the industry, the most common is thermal sealing, whose mechanism involves alumina hydration. However, a high temperature is required, and the slow kinetics of the reaction imply a high energy consumption, leading this method to be replaced by cold sealing mechanisms [13,14]. A recent study proposed the sealing of the AA2524-T3 anodic layer by an organic-inorganic hybrid sol-gel coating, which blocked the pores [15]. Yet, this process involves considerable time and energy expenditure in hydrolysis and condensation reactions. Hu et al. have compared hot and cold nickel sealing, as well as hot water sealing on anodized aluminum and reported a higher corrosion resistance for samples sealed with hot nickel, while samples sealed with cold nickel showed a small advantage over unsealed samples [16]. Other conversion coatings used to improve anticorrosive properties are those based on hexafluorozirconic acid, which are quickly applied by spray-coating or dip-coating directly on metals and have become promising alternatives to phosphate and chromate-based conversion coatings, mainly when used before painting [17–19]. Nevertheless, there are no studies involving the application of these coatings on anodized aluminum alloys. Garcia-Rubio et al. [10] reported that AA2024 samples anodized in TSA and post-treated with Alodine®, a conversion coating containing

Cr(VI) and F⁻, did not show corrosion protection advantages compared to unsealed samples, which suggests that not all conversion coatings have the ability of enhancing corrosion resistance when applied over anodized layers.

This study aims to evaluate the viability of a Zr conversion coating as an alternative post-treatment for anodized AA7075 alloys, applied by the dip-coating method at room temperature. In order to do that, different concentrations and pH values of hexafluorozirconic acid were compared to find an optimum deposition condition. Morphological and chemical analysis were performed by SEM and EDS, respectively. The corrosion resistance was evaluated by electrochemical impedance spectroscopy (EIS). The exposed areas were photographed and compared after 24 days of immersion in NaCl 0.5 M. The behavior of samples covered by the conversion coating was compared to samples sealed with hot water as well as to unsealed samples.

2. Experimental Procedure

2.1 Material

AA7075-T6 aluminum alloy plates, with dimensions of 80 mm × 40 mm × 2.8 mm, acquired from Alrase Metais LTDA, were used for the present work. The composition of the plates was measured by X-ray fluorescence and is shown in Table 1.

2.2 Samples preparation

The plates showed deep scratches on their surfaces when received. Therefore, samples were prepared in order to remove those marks and homogenize the samples, thus guaranteeing the same texture in all of them. Hence, a simple sanding procedure was performed, with #320 and #600 SiC papers, which promoted an intermediate roughness on the surfaces. This step was followed by degreasing with the commercial product Saloclean 667N (Klintex) at 70ºC for 10 min [20], and later rinsing with deionized water and drying with hot air. The next steps of preparation were chosen based in previous works with different aluminum alloys before anodizing [21–23]. It was opted, though, for a longer time and lower temperature of NaOH etching, for practical reasons. The samples were etched in 10% wt. NaOH for 120 s, rinsed in deionized water and then dismutted in 30% wt. HNO_3 for 30 s, both at room temperature. This process was important for the removal of the natural oxide layer and surface homogenization [21].

2.3 Anodizing process

The electrolyte used to perform the anodizing process was a solution of sulfuric acid mixed with tartaric acid: 40 g.L⁻¹ H_2SO_4 + 80 g.L⁻¹ $C_4H_6O_6$ + Arkopal® Surfactant (Sigma-Aldrich) 1 g.L⁻¹. An iCEL PS-5000 model current source was used, applying a current density of 1 A.dm⁻² for 20 min, under constant agitation, at 20 ºC. After anodizing, each sample was rinsed for 1 min inside a beaker with deionized water, under constant agitation, in order to remove acid excess from the pores, and then dried with hot air. For the thermal sealing process, the samples were immersed in boiling deionized water for 20 min, then rinsed with deionized water and dried with hot air.

2.4 Zr-based conversion coating

For the conversion coating, hexafluorozirconic acid (H_2ZrF_6) solutions were prepared from a Sigma Aldrich solution of 50% wt. in H_2O, whose density is 1.51 g.mL⁻¹, and the concentrations obtained were 0.1% wt., 0.5% wt. and 1% wt. of H_2ZrF_6 in H_2O. The pH values were adjusted with NaOH 40 g.L⁻¹ to 2.5, 3, 3.5 and 4 for solutions of 1% wt. H_2ZrF_6 in H_2O, and it was maintained 3.5 for the other concentrations. Immersions were performed by the dip-coating method, using the Marconi MA765 disc lift, for 2 min of immersion, at a rate of 420 mm.min⁻¹ for both immersion and removal, at room temperature. Then, the samples were rinsed with deionized water and dried with hot air. Table 2 shows the different samples produced.

2.5 Oxide and conversion coating characterization

Scanning electron microscopy (SEM) was performed in a JEOL-JSM 6510LV device with an acceleration voltage of 10 keV in order to evaluate morphology and thickness of anodized samples. In addition, SEM images and EDS analyses of top surfaces were performed in a Phenom ProX device with an acceleration voltage of 15 keV.

2.6 Electrochemical impedance spectroscopy

For the electrochemical impedance spectroscopy (EIS) analysis, a naturally aerated NaCl 0.5 M solution was used at room temperature. In each electrochemical cell the exposed area of the sample was 7.07 cm². A KCl saturated Ag/AgCl electrode (+ 0.207 V in relation to the standard hydrogen electrode) was used as reference electrode and a platinum sheet as a counter-electrode. The EIS curves were acquired in a frequency range of 10⁵ Hz to 10⁻² Hz, with an amplitude of

Table 1. % wt. composition of the used alloy

Al	Zn	Mg	Fe	Si
92.096 ± 0.229	5.712 ± 0.062	1.222 ± 0.278	0.291 ± 0.016	0.116 ±0.023
Cu	Zr	Ti	Mn	Cr
0.154 ± 0.007	0.088 ± 0.002	0.052 ± 0.005	0.046 ± 0.012	0.206 ± 0.007

Table 2. Nomenclature of AA7075-T6 samples

Sample	Description
TSA	anodizing in TSA acid without sealing
TSA-HS	anodizing in TSA + hydrothermal sealing
Nano 0.1%	anodizing in TSA + immersion in H_2ZrF_6 1.5 g.L^{-1} pH 3.5
Nano 0.5%	anodizing in TSA + immersion in H_2ZrF_6 7.5 g.L^{-1} pH 3.5
Nano 1.0%	anodizing in TSA + immersion in H_2ZrF_6 15.0 g.L^{-1} pH 3.5
pH 2.5	anodizing in TSA + immersion in H_2ZrF_6 15.0 g.L^{-1} pH 2.5
pH 3.0	anodizing in TSA + immersion in H_2ZrF_6 15.0 g.L^{-1} pH 3.0
pH 3.5	anodizing in TSA + immersion in H_2ZrF_6 15.0 g.L^{-1} pH 3.5
pH 4.0	anodizing in TSA + immersion in H_2ZrF_6 15.0 g.L^{-1} pH 4.0

10 mV (RMS) on the open circuit potential, using an Autolab potentiostat PGSTAT302 and 1.11 version of Nova program. All the analyses were performed in triplicate.

2.7 Fitting of the EIS diagrams with electrical equivalent circuits (EEC)

The quantitative evaluation of the EIS data was performed by fitting the diagrams obtained after 1 h of immersion in NaCl 0.5 M with EEC. The EEC models were determined from the characterization of the different systems and in accordance with the literature. The fitting of the diagrams was carried out with the Nova program.

2.8 NaCl Immersion test

All the anodized samples were immersed in NaCl 0.5 M solution, inside an acrylic cell with an exposed area of 7.07 cm², for 24 days. After that period, the samples were removed from the cells and their exposed areas were photographed to comparison of macroscopic corrosion.

3. Results and Discussion

3.1 TSA anodizing curve for AA7075-T6

Figure 1 shows the curve that describes evolution of potential with time, related to the anodizing of AA7075-T6 in tartaric-sulfuric acid under a constant current density of 1 A.dm^{-2}. The potential achieved 27 V in approximately 20 s, which was the maximum point. This stage is attributed to the dissolution of the Al matrix and to the nucleation of pores. After a typical decay, the potential has stabilized at 23.7 V $\pm$ 0.3, which corresponds to pore growing, i.e., oxide layer thickening [24].

3.2 Morphological and chemical characterization

Top SEM images revealed an inhomogeneous oxide, with irregular pore sizes for AA7075 anodized in TSA (Figure 2 – a). A considerable morphological change was observed after hot-water sealing, showing typical "petal shaped" crystals over the entire surface (Figure 2 – c), which indicates a well-sealed sample [25]. Anodized samples
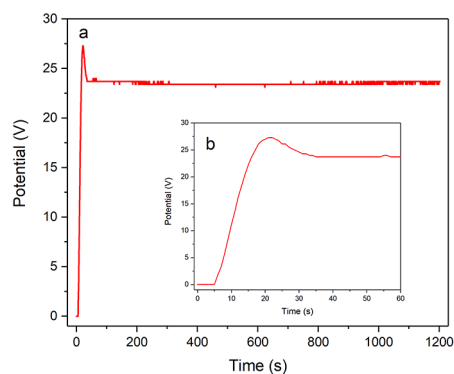

Figure 1. AA 7075-T6 anodizing curve in tartaric-sulfuric acid during 20 min (a) and until 60 s (b).

treated with hexafluorozirconic acid (Figure 2 – b) were also modified and its surface seemed slightly rougher than unsealed samples (Figure 2 – a), analogue to what Garcia-Rubio et al. [10] have found for AA2024 anodized in TSA post-treated with Alodine®, a Cr(VI) conversion coating. They attributed this roughness to an attack caused by some species, as fluoride ions, which would allow chromate ions to react with the alloy surface. The EDS analysis has confirmed the presence of Zr on H_2ZrF_6 treated samples, as shown in Table 3. All TSA-anodized AA7075 samples showed oxygen contents due to the formation of alumina, and the hydrothermally sealed sample showed the highest content due to the hydration of alumina. The samples also showed remnant sulphur, incorporated from the bath.

The cross-section SEM image of the anodized sample post-treated with H_2ZrF_6 (Figure 2 – d) shows an oxide layer with 6.5 $\pm$ 0.6 μm. It was not possible to measure the thickness of the Zr conversion coating over the alumina layer from the micrographs.

As reported by Golru et al. [17], conversion coatings tend to precipitate more on intermetallic particles than on an aluminum matrix. This occurs because of the cathodic behavior played by the majority of intermetallic particles, which turns them into suitable sites for cathodic reactions, thus increasing the local pH upon and around them, allowing a higher deposition of the Zr conversion coating. The same phenomenon occurred for Zr conversion coating on anodized
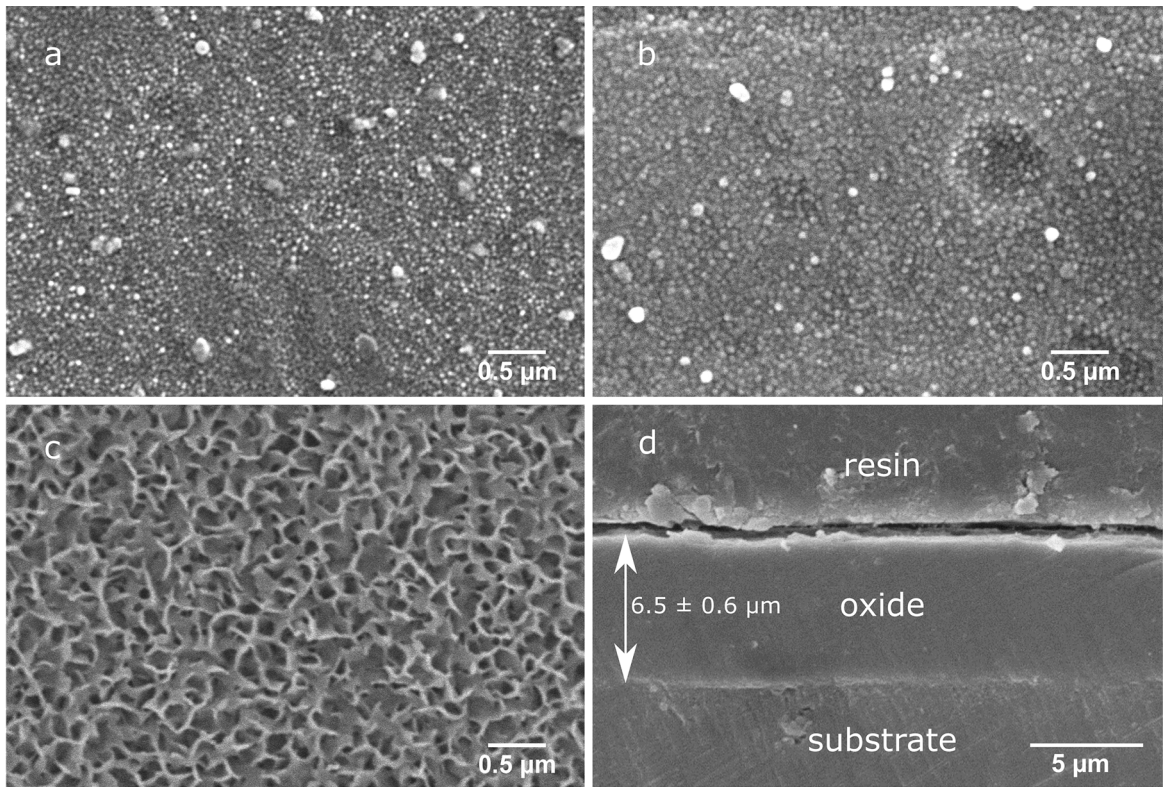
Figure 2. Top SEM images showing the different morphologies of TSA (a), Nano 1.0% (b), TSA-HS (c) and cross-section SEM image of Nano 1.0% sample.

Table 3. Chemical compositions (% wt) of anodized samples obtained by EDS

Element	TSA	TSA-HS	Nano 0.5%	Nano 1%
O	47.49	50.08	34.04	31.38
Al	44.98	43.29	41.28	34.69
S	3.46	3.32	4.05	3.64
Zn	3.58	2.97	3.93	4.97
Mg	0.50	0.33	0.40	0.49
Zr	-	-	14.20	21.34
F	-	-	2.13	2.68

AA7075, which was verified by EDS (Figure 3). The Al-Fe-Si intermetallic region showed a Zr content almost 6 times higher than the matrix region, and no remnant sulphur. Besides, bigger precipitates were visible all over the surface treated with H_2ZrF_6 (Figure 2 – b), which is due to the Zr-oxide precipitation upon the cathodic particles. Hence, one could consider that the nanometric Zr oxide was able to penetrate within the pores' cavities, besides the more intense precipitation upon intermetallic particles.

3.3 Electrochemical impedance spectroscopy

Figure 4 shows Bode plots obtained by EIS after 1 hour of immersion in the NaCl 0.5 M solution. Samples anodized in TSA and coated with Zr oxide exhibited a similar behavior to the samples sealed with boiling water. Two separated time

constants were observed, as occurs to sealed samples [22,24], with displacements in some frequencies. High frequencies are attributed to the most exterior layer, i.e., to the pores edges, while low frequencies are attributed to the barrier layer and middle frequencies are often related to the region within the pores [13,21,25,26]. Hence, as can be interpreted from Figure 4, a sealing mechanism is taking place for anodized samples treated with H_2ZrF_6. It can be proposed that the nanometric Zr oxide plays a role of corrosion inhibitor when applied on the AA7075-T6 anodic layer. Therefore, the decline of impedance in middle frequencies with immersion time for samples with sealing behavior can be associated with the reduction of corrosion protection provided by hydrated alumina (for hydrothermally sealed samples) and by nanometric Zr oxide (for samples subjected to immersion in H_2ZrF_6 solution), in an analogue way.

It was possible to observe that the concentration of the H_2ZrF_6 solution played an important role on the protection of the AA7075-T6 anodized layer, once the solution with the lowest concentration (0.1%) showed a less relevant improvement in the corrosion resistance than the more concentrated ones (Figure 4). Besides, the Nano 0.1% sample showed a less durable protection effect in saline medium: its electrochemical behavior was almost the same as the one of unsealed samples after 24 h (Figure 4 – c, d). Samples subjected to a 0.5% H_2ZrF_6 solution demonstrated a resistance improvement over unsealed samples but had their performance reduced after 408 h of immersion. It should

① Element	%Atomic	%Weight
O	45.79	21.21
Al	30.70	23.99
Zr	17.81	47.04
Fe	3.88	6.28
Si	1.82	1.48

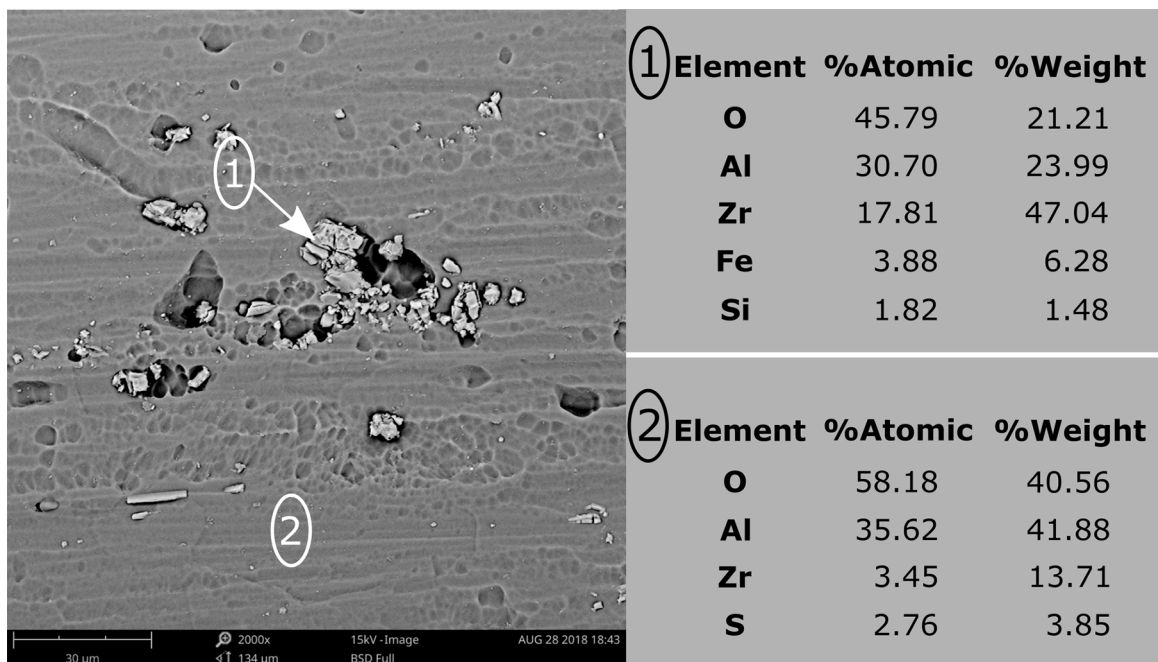| ② Element	%Atomic	%Weight
O	58.18	40.56
Al	35.62	41.88
Zr	3.45	13.71
S	2.76	3.85

Figure 3. Top surface SEM image of nano 1.0% sample showing the precipitates area – 1 – and the matrix area – 2 (a) and its respective chemical compositions (b).

be considered that a flawless barrier layer is not expected to be formed in heterogenous aluminum alloys such as AA7075-T6, mostly because of its intermetallic particles. Thus, low frequencies were not analyzed in terms of coating effectiveness on corrosion resistance.

Figure 5 shows the influence of the immersion time on impedance moduli in 2 middle frequencies for the 5 compared conditions. The Zr-oxide coated samples showed a higher corrosion resistance for longer immersion times in middle frequencies, except for the samples treated by 0.1% solution. Meanwhile, the resistance of samples sealed in boiling water showed a more substantial decrease with the same immersion time. The less concentrated H_2ZrF_6 solution, i.e., 0.1%, provided an ineffective deposition on the anodic layer, since its impedance modulus was almost the same than the unsealed samples. Samples subjected to 0.5% solution showed the highest resistance in middle frequencies, indicating an effective deposition, but its impedance modulus decreased more rapidly in NaCl compared to the 1% solution. However, impedance moduli in middle frequencies for samples treated with 0.5% H_2ZrF_6 were still higher than the ones sealed hydrothermally until 552 h. Samples subjected to immersion in 1% H_2ZrF_6 had the best results as per the impedance diagrams, i.e., they presented the highest values on the Bode modulus diagram, which were higher than values obtained for hydrothermally sealed samples, and had the most separated time constants on Bode phase diagram among the samples treated with H_2ZrF_6, for the longest immersion times in NaCl. Hence, 1% H_2ZrF_6 seems to be the optimum concentration condition for this application within the studied range.

Figure 6 presents the results regarding the influence of pH to the best condition found for H_2ZrF_6 concentration, that is, 1%. The samples subjected to the solution with pH 2.5 had an improvement in middle frequencies, although it was only visible until 1 h in NaCl and then it started to decrease. Besides, these samples showed the lowest impedance values in low frequencies, which were even lower than that observed for unsealed samples. This behavior can be attributed to an intense attack to the bottom of the pores since this solution is more acid and, thus, more aggressive to aluminum oxide, causing the barrier layer to deteriorate fast [25], or even to an attack by the remnant H_2SO_4 from the anodizing bath. So as to discard this last hypothesis, a better acid removal method should be performed after anodizing. Considering the understanding of the deposition mechanism of the conversion coating on anodized aluminum alloys, these were important results. Nevertheless, the behavior in low frequencies shall not be considered to compare the improvement in corrosion resistance obtained by different H_2ZrF_6 treatments, since it is related to the barrier layer, which should be considered the same for all conditions.

Bode diagrams obtained after 1 h of immersion showed similar behaviors for both pH 3 and 3.5 (Figure 6 – a, b). The samples subjected to the solution with pH 3 maintained their impedance values for middle frequencies (Figure 6 – c, d). Figure 7 shows the effect of increasing immersion times on impedance moduli in 2 middle frequencies for the 4 studied pH values. For samples treated with a pH 4 solution, the protection effect has started to decrease after 24 h of immersion in NaCl (Figure 6), which indicates that a less durable deposition is formed in this bath condition. Therefore, a suitable pH range for this application must be from 3 to 3.5.
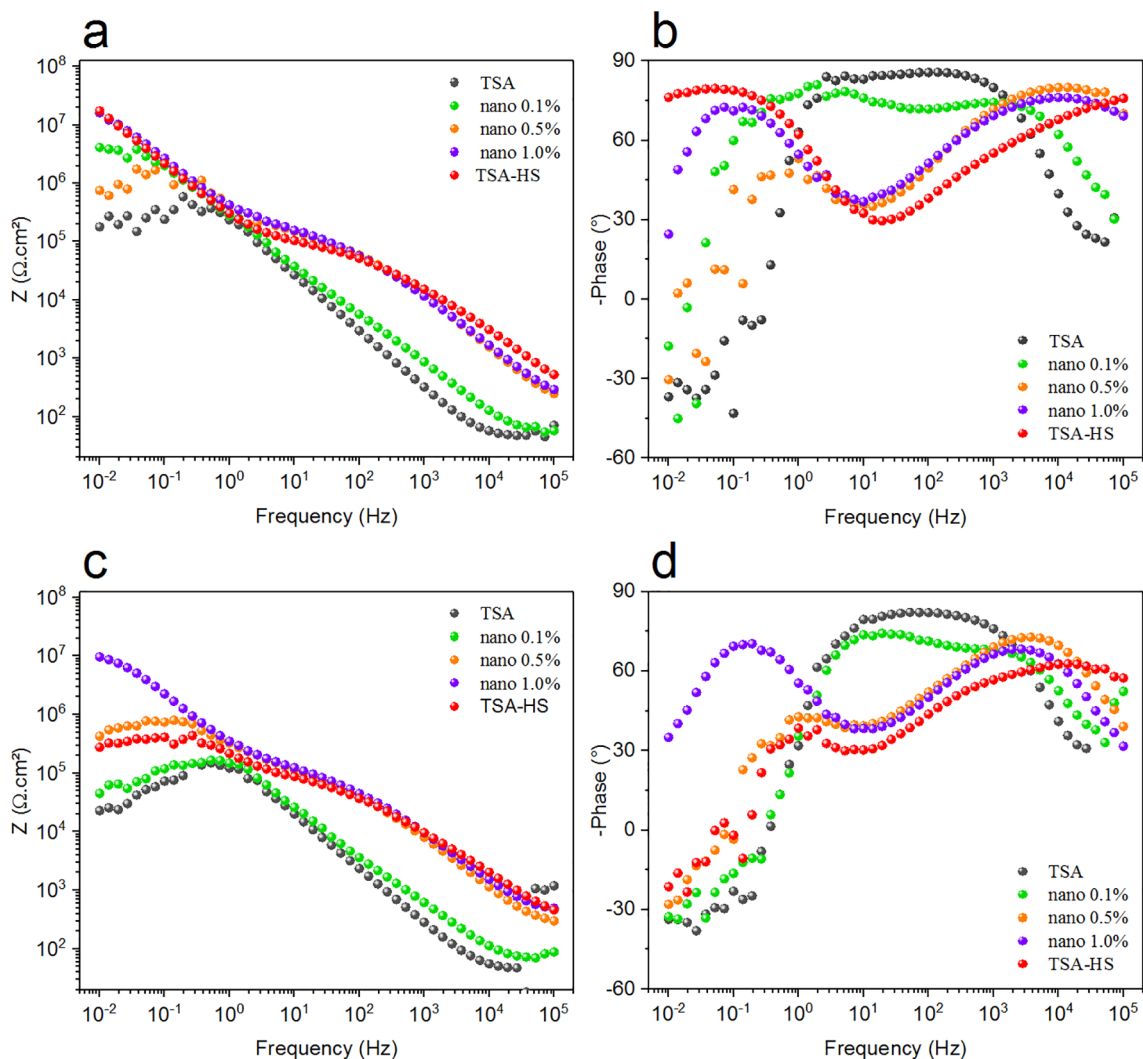
Figure 4. Bode diagrams for anodized samples immersed in H_2ZrF_6 solutions with different concentrations, obtained after 1 h (a – b) and 24 h (c – d) of immersion in NaCl.
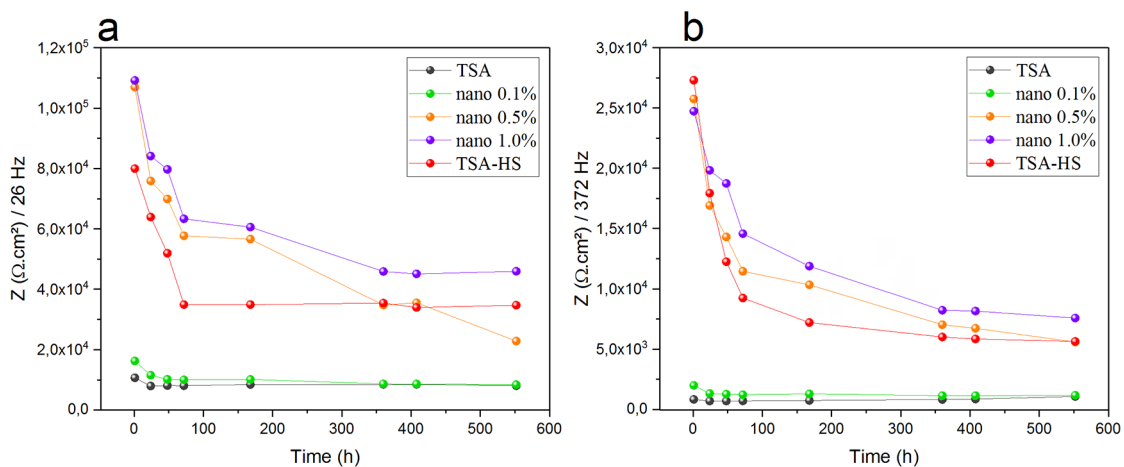

Figure 5. Impedance moduli variation with immersion time in NaCl 0.5 M for 2 middle frequencies: 26 Hz (a) and 372 Hz (b) for anodized samples immersed in H_2ZrF_6 solutions with different concentrations.
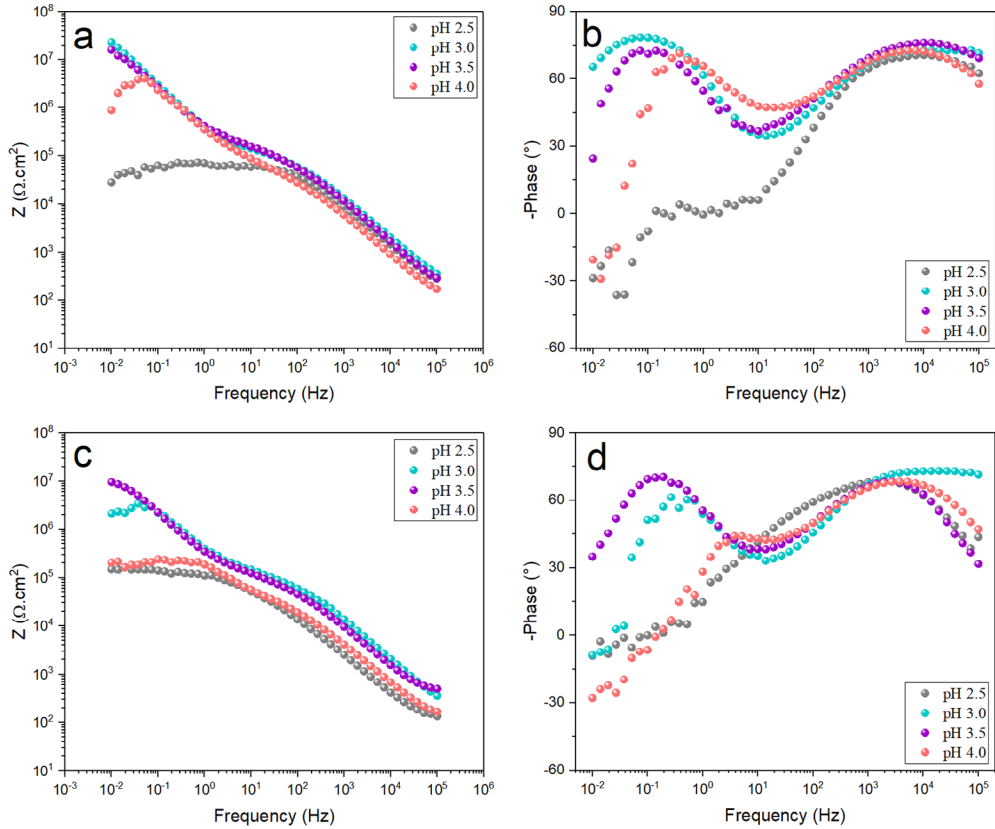
Figure 6. Bode diagrams obtained for anodized samples immersed in H_2ZrF_6 solutions with different pH values after 1 h (a – b) and 24 h (c – d) of immersion in NaCl 0.5 M.
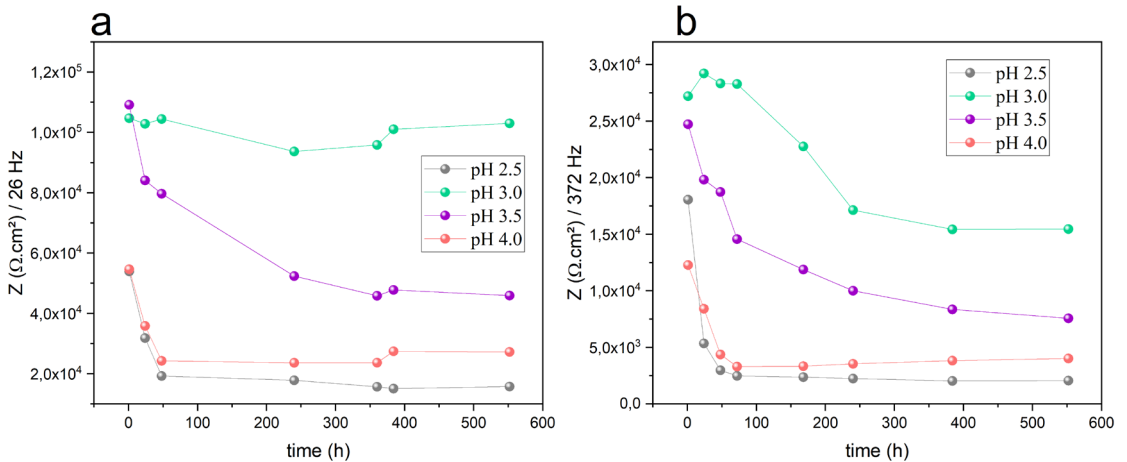

Figure 7. Impedance moduli variation with immersion time in NaCl 0.5 M for 2 middle frequencies: 26 Hz (a) and 372 Hz (b) for anodized samples immersed in H_2ZrF_6 solutions with different pH values.

The observed behavior concerning the pH variation of H_2ZrF_6 bath indicates that the deposition process over anodized AA7075 alloy is pH-conduced, similarly to what different authors have found for this process over bare aluminum alloys [16,17,19]. This similarity can be explained by the fact that the anodized layer over AA7075 alloy is still an aluminum oxide, even though artificially grown, which needs to be slightly dissolved by the acidic solution to increase the

pH locally and initiate the ZrO_2 precipitation. But, if this pH is too low, as 2.5, the anodic oxide will be excessively deteriorated, losing part of its capability of protection instead of anchoring the Zr conversion coating, as it was desired. On the other hand, if the pH is higher than necessary, the solution is not acidic enough to slightly dissolve the anodic oxide to initiate the reaction on the surface and, instead, the ZrO_2 will form and precipitate in the solution bulk [27]. This last situation happened to the H_2ZrF_6 solution with pH 4.

The concentration of H_2ZrF_6 solution is also important to the usability of the Zr conversion coating over anodized AA7075 alloy. Solutions with low concentrations are commonly utilized directly on other substrates [17,19,27] but have now shown to be inappropriate for being used as a corrosion protective on anodized layers. There are studies evaluating corrosion resistance of different conversion coatings based on Zr applied directly on AA7075 alloy [4,19,28]. Nevertheless, the solutions are complex: containing a mixture of many inorganic salts [4] or even commercial baths [28], making it difficult to compare the concentration of each component and its relevance to the deposition mechanism. On the other hand, studies using only H_2ZrF_6 were carried out for other substrates, as galvanized steel [27] and other aluminum alloys [17,19]. Thus, considering the importance of the material composition on the deposition process of conversion coatings, it is possible that AA7075 alloy needs a higher concentration of Zr so that the deposition is possible. Other hypothesis is that a higher concentration is needed to higher aluminum oxide thickness. Since a filling of the porous layer is expected, the interior of these pores corresponds to a larger area for the ZrO_2 precipitation than a simple aluminum oxide, and that would require a higher concentration of Zr in the solution.

3.4 Characterization of protection systems by fitting the EIS diagrams with electrical equivalent circuits (EEC)

As expected, unsealed samples did not show two separated time constants (Figure 4). Instead, they showed a single and wide time constant between low and middle frequencies, visible in Bode phase diagrams. Fig. 8 – a shows a simple scheme of the unsealed porous film and indicates the components of its electrical impedance, which is in accordance with some other schemes in literature [10,16,19-20]. Table 4 shows the values of electrical components, as well as the value of chi-square (x^2). The chi-square values were lower to post-treated systems, indicating a better fitting than that obtained for unsealed system. R_{el} can be related to the electrolyte resistance and, as some authors have suggested [10,26], since it was NaCl 0.5 M, the resistivity is so low that it can be considered the lower value fitted by the Nova program, which was $0.9\ \Omega.cm^2$, for the 3 different systems. R_p is the resistance of the electrolyte in the pores. The capacitive behavior was preferably described as constant phase elements (CPE) rather than pure capacitances, in order to consider the heterogeneity of these layers. Thus, CPE_p is related to the capacitive behavior of the pore walls. The CPE_b is attributed to the barrier layer, in parallel with barrier layer resistance (R_b).

When the sealing process is effective, 2 time constants can be clearly distinguished on the EIS diagrams. One of the constants can be associated with the barrier layer, in low frequencies, and the other with the sealed porous layer, in middle to high frequencies [16,20]. This behavior was expected for samples sealed with boiling water, once

Table 4. Fitted parameters with the EEC from Figure 9 for the EIS diagrams of AA7075 anodized samples

	TSA	TSA-HS	Nano 1%
x^2	0.10	0.018	0.014
Rel ($\Omega.cm^2$)	0.9	0.9	0.9
Rp ($\Omega.cm^2$)	9.43	1.103	15.5.103
Rb ($\Omega.cm^2$)	322.103	22.106	3.60.106
Rf ($\Omega.cm^2$)	-	17.103	180.103
CPEb ($\mu F.cm^{-2}.s(n-1)$)	3.21	4.80	4.29
nb	0.972	0.921	0.966
CPEp ($\mu F.cm^{-2}.s(n-1)$)	0.220	0.223	0.415
np	0.968	0.825	0.833
CPEf ($\mu F.cm^{-2}.s(n-1)$)	-	3.92	12.8
nf	-	0.452	0.45

its morphological characterization indicated a well-sealed surface, i.e., hydrated alumina plugging the pore openings (Figure 2 – c). Figure 8 – b shows schematically its surface structure and equivalent circuit. In Table 4, besides the same parameters of the unsealed samples (R_{el}, R_p, CPE_p, R_b and CPE_b), R_f is a third resistance – a filling resistance – which corresponds to the hydrated alumina precipitated within the pores, plugging them, while CPE_f is the constant phase element related to this third protection mechanism within the pores, parallel to R_f. As it has already been shown by Capelossi et al. [26] and Guadagnin et al.[21], the n value associated to the CPE response of hydrated alumina inside the pores was maintained relatively low because of its porous and complex nature [29]. The R_p value was higher than that obtained for unsealed samples and, when considered together with the value of R_f – resistance of hydrated alumina inside the pores – it was comparable to R_p values from the AA2024 samples anodized in TSA and hydrothermally sealed, according to Boisier et al. [25]. R_b is 3 orders of magnitude higher than R_b from unsealed samples, which was expected regarding this type of sealing.

Although it was not predictable by morphology characterization (Figure 2 – b), the Zr-oxide coated samples showed EIS diagrams typical of sealed samples, namely, with 2 time constants clearly separated. However, the fitting process indicated that the system is composed, in fact, by 3 time constants. This structure is schematized in Figure 8 – c and its electrical components are present in Table 4. Analogue to what happened for hydrothermally sealed samples, R_f is a third resistance, but now attributed to the Zr-oxide coating precipitated within the pores,
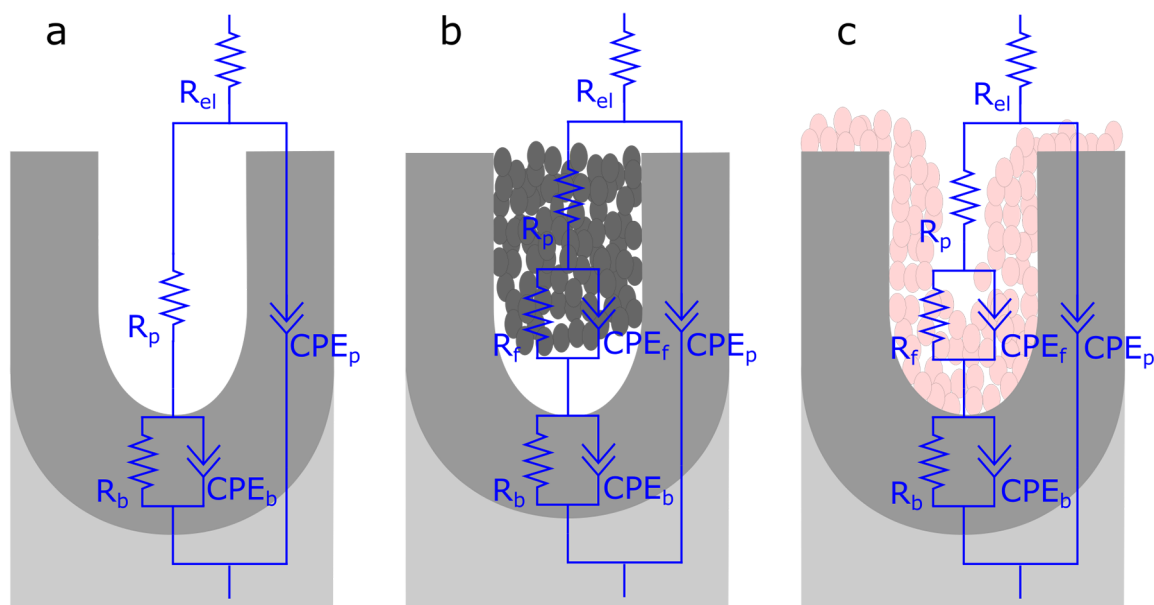
Figure 8. Schemes of the electrical equivalent circuit for 3 different protection systems for AA7075 anodized in TSA: unsealed (a), hydrothermally sealed (b) and protected with Zr conversion coating (c).

which partially fills them. CPE_f is considered its capacitive behavior. The n value was maintained low for the same reason as it was done for the hydrothermal sealing. R_p and R_b had the same order of magnitude as hydrothermally sealed samples. In addition, R_f showed a value more than 10 times higher than R_f from hydrothermal sealing. After 24 h of NaCl exposure none of the samples had showed visible pits on their surfaces, and, as it was evaluated by EIS, samples sealed by boiling water showed a substantial drop in their barrier layer resistance, while samples treated with H_2ZrF_6 were able to sustain their protection (Figure 4). This behavior indicates that Zr-conversion coatings can be used as a protection to the anodic porous layer of aluminum alloys.

3.5 NaCl Immersion test

The sample areas immersed in the NaCl 0.5 M solution were photographed and compared after 24 days of immersion (Figure 9). The unsealed sample showed general corrosion, probably with stable pits underneath its corrosion product (Figure 9 – a). Conversely, the sample sealed in boiling water showed only localized corrosion, that is, some pits, as well as the Zr-oxide covered samples. The sample subjected to 1% H_2ZrF_6 solution showed the lowest number of pits (Figure 9 – c), which was even lower than those observed on the hydrothermally sealed sample (Figure 9 – d). The sample subjected to 0.5% conversion solution showed an intermediate corrosion resistance (Figure 9 – b). These results support the electrochemical results, which indicated a superior corrosion resistance of Zr-oxide covered samples compared to hydrothermally sealed samples.
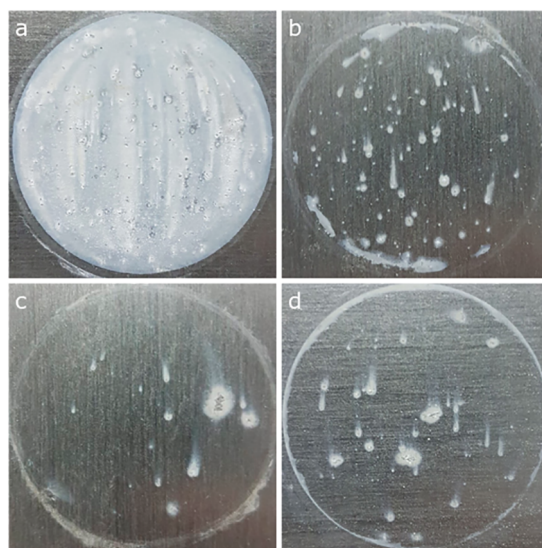

Figure 9. Samples surfaces of TSA (a), Nano 0.5% (b), Nano 1% (c) and TSA-HS (d) after 24 days of immersion in NaCl 0.5 M.

4.Conclusions

A higher corrosion resistance was observed for anodized samples covered with the Zr conversion coating than for the unsealed samples. The best concentration and pH values of the H_2ZrF_6 solution were respectively: 1% wt. (15 g.L^{-1}) and a range from 3 to 3.5. These were the parameters that provided highest and most durable resistance to AA7075-T6 alloy anodized in TSA.

The higher impedance values in middle frequencies indicates that a sealing performance was achieved after the deposition of Zr nanometric oxide on porous alumina layer. Besides, intermetallic particles were preferable sites for precipitation.

The Zr-based conversion coating has proven its ability of acting with the anodized layer of AA7075-T6 alloy as a corrosion protection system free from toxicity and with a higher durability compared to the traditional anodizing system, which is followed by hydrothermal sealing.

5. Acknowledgments

6. References

1. Starke Junior EA, Staley JT. Application of modern aluminum alloys to aircraft. *Progress in Aerospace Sciences*. 1996;32(2-3):131-172.

2. Miera MS, Curioni M, Skeldon P, Thompson GE. Preferential anodic oxidation of second-phase constituents during anodising of AA2024-T3 and AA7075-T6 alloys. *Surface and Interface Analysis*. 2010;42(4):241-246.

3. Zhao J, Xia L, Sehgal A, Lu D, McCreery RL, Frankel GS. Effects of chromate and chromate conversion coatings on corrosion of aluminum alloy 2024-T3. *Surface and Coatings Technology*. 2001;140(1):51-57.

4. Coloma PS, Izagirre U, Belaustegi Y, Jorcin JB, Cano FJ, Lapeña N. Chromium-free conversion coatings based on inorganic salts (Zr/Ti/Mn/Mo) for aluminum alloys used in aircraft applications. *Applied Surface Science*. 2015;345:24-35.

5. European Commission (EC). Press Release - European Commission proposes to ban phosphates in laundry detergents. *European Commission*. 2010.

6. Guo Y, Frankel GS. Characterization of trivalent chromium process coating on AA2024-T3. *Surface and Coatings Technology*. 2012;206(19-20):3895-3902.

7. Qi J, Gao L, Li Y, Wang Z, Thompson GE, Skeldon P. An optimized trivalent chromium conversion coating process for AA2024-T351 alloy. *Journal of The Electrochemical Society*. 2017;164(7):C390-C395.

8. O'Sullivan JP, Wood GC. The morphology and mechanism of formation of porous anodic films on aluminium. *Proceedings of the Royal Society A: Mathematical, Physical and Engineering Sciences*. 1970;317(1531):511-543.

9. Diggle JW, Downie TC, Goulding CW. Anodic oxide films on aluminum. *Chemical Reviews*. 1969;69(3):365-405.

10. García-Rubio M, Lara MP, Ocón P, Diekhoff S, Beneke M, Lavía A, García I. Effect of postreatment on the corrosion behaviour of tartaric–sulphuric anodic films. *Electrochimica Acta*. 2009;54(21):4789-4800.

11. Arenas MA, Conde A, Damborenea JJ. Effect of acid traces on hydrothermal sealing of anodising layers on 2024 aluminium alloy. *Electrochimica Acta*. 2010;55(28):8704-8708.

12. García-Rubio M, Ocón P, Curioni M, Thompson GE, Skeldon P, Lavía A, et al. Degradation of the corrosion resistance of anodic oxide films through immersion in the anodising electrolyte. *Corrosion Science*. 2010;52(7):2219-2227.

13. Gonzalez JA, Lopez V, Otero E, Bautista A, Lizarbe R, Barba C, et al. Overaging of sealed and unsealed aluminium oxide films. *Corrosion Science*. 1997;39(6):1109-118.

14. Zuo Y, Zhao PH, Zhao JM. The influences of sealing methods on corrosion behavior of anodized aluminum alloys in NaCl solutions. *Surface and Coatings Technology*. 2003;166(2):237-242.

15. Costenaro H, Lanzutti A, Paint Y, Fedrizzi L, Terada M, Melo HG, et al. Corrosion resistance of 2524 Al alloy anodized in tartaric-sulphuric acid at different voltages and protected with a TEOS-GPTMS hybrid sol-gel coating. *Surface and Coatings Technology*. 2017;324:438-450.

16. Hu N, Dong X, He X, Browning JF, Schaefer DW. Effect of sealing on the morphology of anodized aluminum oxide. *Corrosion Science*. 2015;97:17-24.

17. Golru SS, Attar MM, Ramezanzadeh B. Morphological analysis and corrosion performance of zirconium based conversion coating on the aluminum alloy 1050. *Journal of Industrial and Engineering Chemistry*. 2015;24:233-244.

18. Andreatta F, Turco A, Graeve I, Terryn H, Wit JHW, Fedrizzi L. SKPFM and SEM study of the deposition mechanism of Zr/Ti based pre-treatment on AA6016 aluminum alloy. *Surface and Coatings Technology*. 2007;201(18):7668-7685.

19. Milošev I, Frankel GS. Review—Conversion Coatings Based on Zirconium and/or Titanium. *Journal of The Electrochemical Society*. 2018;165(3):C127-C144.

20. Moreira VB. Deposição eletroassistida de organossilanos como pré-tratamento para a pintura de substratos metálicos [dissertation]. Porto Alegre (RS): UFRGS - Engenharia de Minas, Metalúrgica e de Materiais; 2016.

21. Guadagnin HC. Corrosion resistance study of AA2524 anodized in sulphuric-tartaric acid and sealed with hybrid coatings [tese]. São Paulo (SP): Universidade de São Paulo; 2017.

22. Curioni M, Miera MS, Skeldon P, Thompson GE, Ferguson J. Macroscopic and local filming behavior of aa2024 t3 aluminum alloy during anodizing in sulfuric acid electrolyte. *Journal of The Electrochemical Society*. 2008;155(8):C387-C395.

23. Miera MS, Curioni M, Skeldon P, Thompson G. Modelling the anodizing behaviour of aluminium alloys in sulphuric acid through alloy analogues. *Corrosion Science*. 2008;50(12):3410-3415.

24. Domingues L, Fernandes JCS, Belo MC, Ferreira MGS, Guerra-Rosa L. Anodising of Al 2024-T3 in a modified sulphuric acid/boric acid bath for aeronautical applications. *Corrosion Science*. 2003;45(1):149-160.

25. Boisier G, Pébère N, Druez C, Villatte M, Suel S. FESEM and EIS study of sealed AA2024 T3 anodized in sulfuric acid electrolytes: Influence of Tartaric Acid. *Journal of The Electrochemical Society*. 2008;155(11):C521-C529.

26. Capelossi VR, Poelman M, Recloux I, Hernandez RPB, Melo HG, Olivier MG. Corrosion protection of clad 2024 aluminum alloy anodized in tartaric-sulfuric acid bath and protected with hybrid sol–gel coating. *Electrochimica Acta*. 2014;124:69-79.

27. Cardoso HRP, Rapacki C, Ferreira JZ. Monitoring of a Zr-based conversion coating on galvanised steel and its performance against corrosion. *Corrosion Engineering, Science and Technology*. 2019;54(8):726-730.

28. Li L, Whitman BW, Munson CA, Estrada R, Matzdorf CA, Swain GM. Structure and corrosion performance of a non-chromium process (NCP) Zr/Zn pretreatment conversion coating on aluminum alloys. *Journal of The Electrochemical Society*. 2016;163(13):C718-C728.

29. Boisier G, Lamure A, Pébère N, Portail N, Villatte M. Corrosion protection of AA2024 sealed anodic layers using the hydrophobic properties of carboxylic acids. *Surface and Coatings Technology*. 2009;203(22):3420-3426.